Joint Centre for Mesoscale Meteorology, Reading, UK

The effects of convection on chemical reactions and precipitation scavenging

N. R. Gimson

Internal Report No. 90

July 1998

Met Office Joint Centre for Mesoscale Meteorology Department of Meteorology
University of Reading PO Box 243 Reading RG6 6BB United Kingdom
Tel: +44 (0)118 931 8425 Fax: +44 (0)118 931 8791
www.metoffice.com

Designed and produced by the Met Office © Crown copyright 2001 01/0240 The Met Office logo is a registered trademark.

The effects of convection on chemical reactions and precipitation scavenging

Neil R. Gimson*

JCMM, Department of Meteorology, University of Reading, UK.

14 July, 1998

Summary

The effects of cumulus convection on the dispersion and removal of chemically active species are considered in the framework of a mesoscale model. The subgrid-scale clouds are parametrized, according to a "mass-flux" scheme, with chemical species having both in-cloud and environmental components.

A simple reaction scheme is applied, consisting of a localized NO_x emission, which is oxidized in the presence of ozone and the hydroxyl radical to $N(v)$ species, which themselves are scavenged by precipitation and deposited at the surface.

A case of maritime convection around the United Kingdom is studied (23 October, 1992), which was widespread over the Atlantic Ocean, Irish Sea and the North Sea, but also penetrating inland during the daytime. The dispersion from idealized NO_x emissions is studied, and subsequent transformations and removal examined, in terms of the lifetimes of chemical species, under the influence of convection, diffusion, reaction and removal. A mid-level source of NO_x produces a plume which travels eastwards over the British Isles, oxidizing first at its leading edge - the oldest portion. Despite the variation in oxidation rate with height, domain totals of NO_x and $N(v)$ are altered only slightly by the presence of convective effects, since convective time-scales are generally shorter than the times of the chemical reactions used here. However, significant reduction in the rate of oxidation occurs in some locations of the computational domain in the final few hours of the integration.

Scavenging of $N(v)$ is affected by convection, chiefly because stratiform and convective rain fall at different locations. More $N(v)$ is washed out when convective effects on the chemical species are included, much over the sea, and the sub-gridscale removal concentrates the deposition into a smaller area.

Though somewhat idealized, the numerical simulations demonstrate important interactions between chemistry and convection, and show that convective effects should be incorporated into a atmospheric chemistry model for the realistic representation of these interactions.

* *Address for correspondence:* Dr. Neil R. Gimson, NIWA Research Ltd., Box 109695, Newmarket, Auckland, New Zealand. E-mail address: n.gimson@niwa.cri.nz.

1 Introduction

It is well known that cumulus clouds can have a dramatic effect on the vertical redistribution of tracers, and on their subsequent dispersion. Rapid updraughts may raise pollutants through many kilometres in tens of minutes, to levels where the wind velocity may be different, where lower temperatures lead to slower reaction rates and longer primary pollutant residence times, where the incoming solar energy varies, affecting photo-chemistry, and where ambient reactant concentrations are different. Evaporatively-cooled downdraughts can be effective in bringing tracers from the middle troposphere to the surface levels, and associated precipitation in bringing hygroscopically-controlled contaminants to the surface itself, both of these mechanisms serving to pollute the boundary layer with, for instance, acidic precipitation or radioactive fallout. This may have consequences for plants, livestock and humans.

To focus on specific trace species, it is known, from combinations of aircraft observational campaigns and modelling studies, that convection increases the atmospheric residence time of ozone (O_3) by transporting ozone and its precursors, oxides of nitrogen (NO_x) and volatile organic compounds (*VOC*), out of the boundary layer (Pickering *et al.*, 1992; Ridley *et al.*, 1994; Lelieveld and Crutzen, 1994; Elliott *et al.*, 1996). In the free troposphere, ozone production efficiency is higher, chemical losses are slower and there is no surface deposition. This has consequences for the long-range transport of ozone, leading to elevated concentrations at high altitudes downwind of an urban area (see for example, Thompson *et al.*, 1994). In addition, ozone is more effective as a greenhouse gas at higher levels. Convection may also reduce lower-troposphere ozone concentrations during ozone episodes (Hov and Flatøy, 1997).

Given the evidence for increased amounts and prolonged lifetimes of secondary pollutants it is still difficult to ascertain precisely the mechanisms by which they result. They may be, for the case of ozone,

- the vertical transport of ozone in convective updraughts,

- the vertical transport of boundary-layer precursor species to levels of increased ozone production efficiency at a different temperature or solar radiation levels, or
- the vertical transport of precursors to levels of higher concentrations of other reactants, leading to higher concentrations of the product, ozone.

The production and fate of the secondary pollutant, ozone, is beyond the scope of this paper, but since it results from complex, non-linear chemical reactions involving precursor oxides of nitrogen, the effects of convection upon the vertical distribution of NO_x are examined here. Also under consideration are the effects of convection on scavenging and deposition, which are expected to be significant (Tremblay, 1987; Yuen *et al.*, 1996).

To give a realistic description of local air quality or long range transport, a numerical model must thus include a representation of cumulus convection. Many sophisticated chemistry modules are available for use in one-dimensional cloud models (Walcek and Taylor, 1986; Hong and Carmichael, 1986; Cho *et al.*, 1989). Various three-dimensional cloud-chemistry models are also in existence where individual clouds are resolved by the model (for example, Tremblay and Leighton, 1986; Tremblay, 1987; Niewiadomski, 1989; Wang and Chang, 1993(a,b); Leighton *et al.*, 1996). For long-range dispersion, chemical schemes in regional models may operate as a post-processing step on given meteorological data, and may include some parametrization of cumulus effects (Chang *et al.*, 1987; Berkowitz *et al.*, 1989; Carmichael *et al.*, 1991; Karamchandani and Venkatram, 1992; Lin *et al.*, 1994). This presents a challenge, and on the mesoscale, it is essential that the effects of convection are parametrized. The parametrization involves the derivation of properties of the convective clouds themselves, such as mass fluxes, cloud cover and water content, but must be expressible in terms of the 'resolved' meteorological fields. This is referred to as the "closure" problem. The parametrization scheme redistributes the resolved fields such as momentum, heat, moisture and chemical tracer concentrations in the vertical, through the influence of the sub-gridscale cumulus clouds.

In a mesoscale forecasting model, with horizontal resolution 15 km, Gimson (1997) considered the effects of the sub-gridscale cumulus clouds on releases of inert tracers, by developing suitable schemes for their vertical redistribution. For an episode of mid-latitude, mid-level, maritime convection, a rapid vertical spread of the tracer plume was found, both to the surface and cloud top levels. Also, turbulence and convection were found to interact, so as to enhance the upward transport of pollutants, by diffusion of a low level plume up through the boundary layer, and allowing subsequent convective transport to the cloud top level. Surface-level concentrations, resulting from downward transport were decreased by turbulent mixing in the boundary layer, which eroded the maximum at the lowest levels. More details on mass-flux convective parametrization schemes, and the effects of cumulus on conserved tracers are given in the introduction of Gimson (1997). This paper presents a continuation of that work, investigating the consequences for some chemically reactive and hygroscopic species. The focus of this work is the possible effects of convection on chemical transformations, and hence as simple a chemistry model as possible is employed. This includes only a few species - gaseous oxides of nitrogen, nitric acid gas and particulate nitrate. Nevertheless, even in the reduced chemical mechanism used, the chemical species are subject to photo-chemistry, altitude-dependent reaction rates and scavenging.

The chemical scheme used here contains a subset of the reactions used in the EMEP (European Monitoring and Evaluation Programme) scheme (Sandnes, 1993; Derwent, 1990, 1993), to incorporate emissions of NO_x, oxidation to nitrates and precipitation scavenging of nitrates. Realistic reaction rates are used and the mesoscale meteorology is fully described - the cloud-scale meteorology is, of course, parametrized. Solving simultaneously for meteorology and pollutant dispersion provides detailed meteorological data, every minute, at mesoscale resolution, upon which the chemistry and scavenging sub-model depend. Then, effects of ensembles of cumuli on transport, diffusion, transformation and removal, the relative importance of these processes with and without convective effects on the pollutants, and the interactions of cloud dynamical effects with those due to the rest of the atmospheric dynamics may be determined.

Section 2 describes the chemistry and precipitation scavenging schemes and their relation to the cumulus parametrization, and section 3 contains results from integrations of the mesoscale model with an actual forecast case and idealized emissions. The work is summarized and avenues for future investigation are discussed in section 4.

2 The chemistry and precipitation scavenging models

The evolution of a chemical species is described by the generic equation

$$\frac{\partial \chi}{\partial t} + \nabla.(\mathbf{u}\chi) = S_c(\chi_1, \chi_2) + S_d(\chi) + S_r(\chi)$$

Equation 1

χ is the grid-mean species concentration, **u** the model-generated velocity field, ∇ is the three-dimensional gradient operator in (x, y, η) -co-ordinates where η is the height above the surface, and the right hand side contains sources and sinks due to convection (S_c) and turbulent diffusion (S_d) acting on the grid-mean concentration. The reader is referred to Gimson (1994) and Gimson (1997) for derivations of these terms. The sub-gridscale components of χ are given the subscript j, equal to 1 or 2 for updraught or downdraught respectively, and their evolution is described by the equation

$$\frac{\partial \chi_j}{\partial t} = S_{c,j} + S_{r,j}(\chi_j) \qquad j = 1,2,$$

Equation 2

where $S_{c,j}$ represents schematically the in-cloud convective flux and mixing with the environment (see Gimson (1997), equation (15)). S_c and $S_{c,j}$ are closely related. Terms in S_r are new. They denote emissions, chemical

reactions and removal, and differ between species and between in-cloud and cloud-environment components.

Chemistry and scavenging routines are implemented, based on the EMEP scheme (Sandnes, 1993) for oxides of nitrogen, in the presence of prescribed concentrations of ozone, O_3, and the hydroxyl radical, OH* . A localized emission of NO_x is envisaged, comprising NO and NO_2 in chemical equilibrium. NO_2 experiences a small amount of dry deposition over land, but is oxidized to particulate nitrate at night in the presence of O_3, and to nitric acid, HNO_3, by day in the presence of OH. The products are both readily scavenged by precipitation. To simplify the model it is assumed that both are removed at the same rate, and hence may be represented by one dependent variable, labelled $N(v)$, as the nitrogen has oxidation number five.

Thus, Equation 1 and Equation 2 each apply to two variables, such that χ is $[NO_x]$ or $[N(v)]$, and χ_j is $[NO_x]_j$ or $[N(v)]_j$, for j=1 or 2. The square bracket denotes concentration. Hence $[NO_x] = [NO] + [NO_2]$ and $[N(v)] = [NO_3] + [HNO_3]$. S_c, S_{cj} and S_d operate on $[NO_x]$ and $[N(v)]$ in the same way for each. Chemical reactions and removal may be expressed as

$$S_r([NO_x]) = S_e - \frac{1}{\tau_a}[NO_x] - \frac{1}{\tau_b}[NO_x]$$

$$S_r([NO_x]_j) = S_e - \frac{1}{\tau_a}[NO_x]_j - \frac{1}{\tau_b}[NO_x]_j$$

* It should be noted that this is the chemical mechanism described by Sandnes (1993). Work by Derwent (1990, 1993) refers to a chemical mechanism in the EMEP model in which ozone is *predicted*. The present paper refers, it appears, to a somewhat simplified version of the EMEP chemical mechanism, though no distinction between versions has been found in the literature. This work only considers part of the chemical mechanism, neglecting the chemistry of peroxyacetyl nitrate, ammonia, ammonium salts and sulphur-containing salts. In this simplified version it is desirable to ascribe to the ozone concentration a realistic value, since it depends on, in addition to NO_x, complex non-linear reactions involving volatile organic compounds. Considering only the chemical equilibrium of NO_x and O_3 severely underestimates the ozone concentration.

$$S_r([N(v)]) = \frac{1}{\tau_a}[NO_x] - \frac{1}{\tau_d}[N(v)] - \sigma$$

$$S_r([N(v)]_j) = \frac{1}{\tau_a}[NO_x]_j - \frac{1}{\tau_d}[N(v)]_j - \sigma_j .$$

A full derivation of S_e and the τ's is given in Appendix A. Time scales τ_b and τ_d are for dry deposition, which turn out to be very large; τ_a represents the time scale of the change to NO_x due to the oxidation of NO_2 to *N(v)*; σ and σ_j denote grid-mean and in-cloud precipitation scavenging of *N(v)*. The oxidation terms are height-dependent, as they depend on temperature, $[O_3]$ and $[OH]$, which themselves vary with altitude. Also, being photo-chemical they depend on the time of day. Inspection of the reaction mechanisms described in Appendix A indicates that with the slower formation of NO_2* at altitude, the $[NO_2]/[NO]$ ratio decreases by a factor of three between heights 500*m* and 4000*m* during daytime. The oxidation rate of NO_2 decreases by a factor about four between these levels, hence a net reduction in the NO_x to *N(v)* reaction rate is indicated through the effects of convective updraughts. However, these estimates refer to in-cloud conditions only, and grid-averaged effects over the 18-hour integration are less easy to predict.

When the convective redistribution scheme is in operation, that is $S_c \neq 0$, the S_r-equations have the same form for both in-cloud and environmental (that is, the remaining area of the model grid cell) components of the chemical species, with the exception of the scavenging terms.

Removal by precipitation is represented by σ. The mesoscale model carries both dynamic and convective rainfall types, and σ differs accordingly between in-cloud and environment areas. Dynamic precipitation scavenges environmental *N(v)* and convective precipitation scavenges in-cloud *N(v)*. The large-eddy simulation in Gimson (1997) demonstrated rainfall in both convective updraughts and downdraughts, hence *N(v)* is removed from each of these components. A simple scavenging ratio formulation is used. Its

* Formation of NO_2 occurs through reaction of *NO* with ozone. Reducing this reaction rate leads to higher ozone concentrations at higher altitudes.

appropriateness is arguable in a mesoscale model, as it represents a long-term average of chemical concentrations in rainwater and air and is generally used as a measure of conditions near the surface. However, it suffices for the idealized conditions simulated here.

Introducing A_1, A_2 and A_3, the updraught, downdraught and environment areas, where the grid area $A = A_1 + A_2 + A_3$, the environment concentration $[N(v)]_3$ of $N(v)$ is diagnosed from the relation

$$A\,[N(v)] = A_1\,[N(v)]_1 + A_2\,[N(v)]_2 + A_3\,[N(v)]_3,$$

where $[N(v)]$, $[N(v)]_1$ and $[N(v)]_2$ are calculated deterministically from Equation 1 and Equation 2. Subscript j=3 refers to the environment, not occupied by up- or down-draught. The time scales, τ_j, for removal are given by

$$\frac{1}{\tau_1} = \frac{0.9 p_{conv} \Lambda_v}{\rho_w h_1}, \quad \frac{1}{\tau_2} = \frac{0.5 p_{conv} \Lambda_v}{\rho_w h_2} \text{ and } \frac{1}{\tau_3} = \frac{p_{dyn} \Lambda_v}{\rho_w h_3},$$

where p_{conv} and p_{dyn} are the convective and dynamic precipitation rates in mm s^{-1}, ρ_w is the density of water, and h_j are height scales for removal, which are measures of the cloud and plume overlap distance. The scavenging ratio for $N(v)$, Λ_v, is the ratio of concentration in water to concentration in air. For gases, this is closely related to the Henry's law constant, and here is equal to 1.4×10^6. Constant factors are included to represent the fraction of the up- and down-draughts containing convective rain. Appendix B shows the derivation of τ_j and h_j. Removal terms are given by

$$\sigma_j = \frac{[N(v)]_j}{\tau_j}, \text{ for } j = 1, 2 \text{ or } 3,$$

with

$$\sigma = \frac{1}{A}\left(A_1\sigma_1 + A_2\sigma_2 + A_3\sigma_3\right).$$

3 Results

3.1 Meteorological conditions

The meteorological data are supplied by the United Kingdom Met. Office non-hydrostatic mesoscale model (see Golding (1990)), which re-runs an 18 hour forecast over the British Isles from midnight on 23rd October, 1992. The model horizontal resolution is 15 km, on 32 η -levels. The meteorological model and the pollutant dispersion schemes are run simultaneously, with a time step of 1 minute. During this period there was widespread convection over the British Isles and surrounding seas, in the air behind a cold front which had passed through during the previous day.

The essential meteorological features may be obtained from the model forecast data for midday, in Figure 1. The horizontal velocity field 1500 m above sea-level shows west and north westerly flow over most of the area, with maximum speed 25 m s^{-1}. To the east, the flow is slower and turns northwards over the North Sea. The more rapid southerly flow in the NE corner of the domain is associated with a small-scale trough. This picture changes little with time, except that the main westerlies penetrate further east, and the cyclonic flow in the NE becoming more stagnant over the central North Sea. The picture is similar at the other levels, apart from an increase in wind speed with height, and a westward tilting with height of the trough feature.

The convective cloud top height is also shown for the same time, outlining where the convectively active regions are. These are mainly over the sea, with some penetration eastwards inland over Ireland, Wales and NW-England. The height varies between 3 and 5 km, and the cloud cover is on average about 10%. The convection is most widespread during the day, increasing from dawn and decreasing in extent after dusk. Cloud base levels are generally between 1 and 1.5 km. The features to note, then, which are

important for pollutant dispersion are a general westerly flow, stagnation over the North Sea, and maritime mid-level convection, reaching maximum activity in the afternoon.

The implementation of the sub-gridscale convective transport scheme for airborne tracers is described by Gimson (1997, section 4(a)). Numerical experiments are carried out with hypothetical sources of pollution, the different runs including or omitting convective effects and scavenging, as shown in Table 1. Convective effects on momentum, heat and moisture are always included in the meteorological model runs. All runs are subject to turbulent diffusion and dry deposition, and are based on a localized emission of NO_x, ellipsoidal in shape, with a horizontal radius 60 km, vertical diameter 1000 m , and smooth edges, centred at a height 1500 m above the surface. The source is located over Northern Ireland, simply as this is a location over land, and upstream of convective activity. It is also idealistically placed at a level so as to intersect the convective cloud base, which usually near the top of the boundary layer. To be more realistic, surface-level releases would disperse vertically until they intersect the convective-cloud base. This stage is circumvented. For the EMEP grid square containing this region, the average surface NO_x emission rate is given by Sandnes (1993) as 883 mg(N) m^{-2} $year^{-1}$, converting to 0.63 kg(N) s^{-1} in the 150x150 km^2 area. Letting this be due to the single source described above, its central amplitude is 3.7×10^{-4} μg(N) m^{-3} s^{-1}.

Run number	Convective effects on pollutants	Scavenging of N(v) species
C6	No	No
C7	Yes	No
C8	No	Yes
C9	Yes	Yes

Table 1: Details of the numerical runs.

The four numerical runs are described in the following sections, in order to study the effects of convective transport of pollutants on their chemical

lifetimes, and the effects of scavenging by convective rain on the surface deposition. Hence runs *C6* and *C7* are compared, followed by *C8* and *C9*.

3.2 Run C6: Transport by the 'resolved' flow

Run *C6* contains neither subgrid convective transport nor precipitation scavenging of *N(v)*. The domain totals, in terms of nitrogen mass are shown in Figure 2, against the time in hours after midnight on 23 October. The curves are all generally increasing with time, and their sum is consistent with the constant emission rate. Before dawn, about 0800h, the NO_x and NO_2 curves coincide, as there is no photolysis of NO_2 to *NO*. During the day, from 0800h to about 1630h, photolysis does occur, $[NO_2]$ is less than $[NO_x]$ and some *NO* is thus present. Near dusk, the transformation of *NO* to NO_2 starts to dominate, until, after dark, the NO_x is again all NO_2.

By night, NO_2 oxidizes to *N(v)* through reactions involving ozone, which accelerate in time as the NO_x plume diffuses down to levels with higher $[O_3]$. At dawn, the reaction mechanism changes to that involving the hydroxyl radical, and proceeds at a slower rate. By dusk, the O_3 reaction takes over again, and is more rapid at this time than at dawn, as dusk is warmer and reaction rates are faster.

Information on the vertical motion of the pollutant plume as a whole may be obtained from vertical profiles of the horizontally integrated chemical species. These are shown in Figure 3. The concentration of NO_x at the source level increases monotonically in the morning, as the emission rate dominates other effects (Figure 3(a)). Later however, it decreases quite rapidly - the peak concentration at 1500h is less than at 1200h - turbulence disperses the NO_x downwards and it is also lost in the formation of *N(v)*. Diffusion leads to a rapid increase in $[NO_x]$ below the source level between 1200h and 1500h. By the end of the integration, at 1800h, diffusion effects are not so large and the peak $[NO_x]$ at 1500 m is restored. However, the chemical losses of NO_x continue and, being more rapid nearer the surface, lead to a decrease in $[NO_x]$ values at low levels in the last three hours. To further show the importance of chemistry in this run, a similar integration has

been carried out, containing only emissions of an inert tracer. There, the peak at 1500h is restored more quickly during the day, and low-level concentrations are always increasing.

The oxidation products, denoted *N(v)*, are shown in Figure 3(b). As there are no chemical losses to *N(v)*, turbulent diffusion is a dominating effect, spreading *N(v)* both up- and down-wards. Sinks due to diffusion from the source level can balance sources due to chemical production of *N(v)* as peak values of [*N(v)*] at 1200h and 1500h are quite similar. A fairly well mixed layer is produced through mixing from the boundary layer top, with an increase at the lowest levels of [*N(v)*] through the additional effect of chemical sources of *N(v)* at these warmer levels.

Thus it is seen that vertical diffusion and chemical sinks can balance sources due to emissions. Also, the vertical diffusion tends to produce a well-mixed layer of uniform concentration, in spite of the source being non-uniform in height.

Although convective effects on the chemical species are not included in this run, the parametrization is operational in the meteorological part of the model, and its effect on the 'mean flow' variables is unavoidable. This accounts for the maximum in *N(v)* at 1500h and 1800h at the convective cloud base level. It is due to environmental subsidence transporting the pollutants down to this level. A maximum also occurs at this level in the inert tracer case.

To demonstrate the extent and development of the chemical plume in the horizontal it is meaningful to present the column-averaged distributions of NO_x and *N(v)*. An indication of the vertical spread is given by the vertical concentration profiles in these runs and the effect of convection on tracer dispersion is considered in greater depth elsewhere (Gimson, 1997). The NO_x plume extends from its source region over Northern Ireland, eastwards over the Irish Sea. By 0600h it reaches the north of England (Figure 4(a)). The change in wind direction from the north-westerlies over the western part of the domain, to the southerly direction over the North Sea, leads to a

distortion of the NO_x plume. By 1200h (Figure 4(b)), the leading edge of the plume has travelled across England and on to the North Sea, whereas the rest travels to the south-east. After 18 hours, the north-westerly winds are further inland, taking the most recently emitted pollutants over the mainland, while the oldest part of the plume is roughly stationary over the North Sea (Figure 4(c)).

Inspection of Equation 1 shows that losses of a chemical species from, say, its initial level are due to vertical advection, turbulent diffusion, convective transport, and chemistry. The first two of these do not affect the column average and convective tracer transport is not in operation, thus the only 'non-conservative' changes to the NO_x plume are due to chemical reactions. The eastern portion of the plume is affected by chemistry the most, and the leading edge of the plume has lower values than those around the source region. After 18 hours of integration, the amount of NO_x over the North Sea is far less than over the source region - and decreases along the plume.

For a given value of $[O_3]$ at 1500 m and a temperature of 273K, the oxidation time-scale for NO_x to *N(v)* is about 6 hours. Significant amounts of *N(v)* are thus not visible immediately. Figure 5(a) shows the column-averaged *N(v)* after 6 hours. The maximum in $[N(v)]$ is co-located with the leading end of the NO_x plume, and elsewhere $[N(v)]$ is less than $[NO_x]$. This continues (see Figure 5(b) and (c)) until finally the plume has a maximum $[N(v)]$ over the North Sea, and a far smaller concentration over Northern Ireland. In Figure 5(c), $[N(v)]$ is greater than $[NO_x]$ over the North Sea, even though the domain total amount of *N(v)* is less than the total $[NO_x]$ at this time.

As the transformation in air from NO_x to *N(v)* is gradual, with time-scales of the order of hours, it is to be expected that convection dominates chemical processes locally. For an updraught of, say, 4 ms^{-1} over a cloud depth of 3500 m , the convective transport time-scale is 15 minutes, compared to the oxidation time-scale of 6 hours. This contrast in time-scales may be offset by the partial cloud cover within a grid area, and also the partial domain coverage of the convection itself. Run *C6* is repeated with the convective transport scheme for chemical tracers in operation.

3.3 Run C7: The effect of convective transport on chemical lifetimes

When the convective parametrization is applied to the chemical species it is expected that (a) NO_2 reacts to produce $N(v)$ more slowly, as $[OH]$ and temperature decrease with height and convective updraughts raise the NO_2 from its initial levels, and (b) NO reacts to produce NO_2 more slowly at altitude during the day, due to the vertical variation of ozone. The net effect on $[NO_2]$ may be either an increase or a decrease. These effects turn out to be small for the reactions investigated in this paper. That is, domain totals - shown for run *C6* in Figure 2 - are not changed significantly by the effects of convective transport, in the absence of precipitation scavenging. In fact, the chemical reactions chosen for this model are slow compared to convective transport, the vertical spread due to convection is both up- and down-wards to levels of both slower and faster reaction, only a part of the original plume is displaced from its original level by convection, and the height variation of temperature, $[OH]$ and $[O_3]$ are not large.

Although the domain-total amounts of NO_x and $N(v)$ are changed little by convective effects on the pollutants, local concentrations are affected more noticeably. Profiles of NO_x for run *C7* are shown in Figure 6(a), and demonstrate similar trends to those in Figure 3(a). The additional effect here is the convective transport of NO_x, which further erodes the 1500 m values of $[NO_x]$, particularly in the afternoon. This maximum in concentration also takes longer to restore after its daytime decrease; convective activity is at its most intense in the afternoon. Significant amounts of NO_x are lifted to the cloud top levels, between 4 km and 5 km ; the source level is near to the cloud base level, where the entrainment rate into the cloud is largest. Between 1500h and 1800h there is little increase in $[NO_x]$ above the source levels. The chemical sink of NO_x at cloud-top levels happens to be in balance with a source from convective uplifting, as the convective activity continues during these times.

Below the source level, a maximum in $[NO_x]$ develops near the surface with higher values than those in run *C6*, as the convective downdraughts all

extend down to η= 255 m. Between this level and the source level, [NO_x] is less in run *C7* than in run *C6*, as there are convective cloud base levels in this range, entraining contaminants into the clouds to be transported upwards. Chemistry is still important below the source level, as [NO_x] is again less at 1800h than at 1500h.

Figure 6(b) shows profiles of [*N(v)*]. At the source level, [*N(v)*] remains constant from 0600h to 1500h, a longer period than in run *C6*, and at a lower value. The daytime convective activity acts to spread the *N(v)* in both vertical directions, leading to local maxima both near the surface and at cloud-top levels. These profiles must result from either convective transport of the oxidized species (*N(v)*) or the oxidation of NO_2 at its new levels. However, since NO_x is nearly constant at upper levels between 1500h and 1800h, the reaction time-scale and convection time-scale must be similar, as one cancels the other. The *N(v)* profiles are therefore due to both processes similarly, which are both sources of *N(v)*. At levels near the surface, the decrease in [NO_x] is accompanied by an increase in [*N(v)*] between 1500h and 1800h, indicating the dominance of chemistry there.

Thus the evolution of the vertical structures of NO_x and *N(v)* are greatly affected by the convective transport of the species, with a complex interaction between chemical and convective processes. The detailed examination of Figure 3 and Figure 6 presented here attests to this.

To investigate the local effects of convection on chemical lifetimes, it is instructive to compare vertically integrated chemical distributions with those obtained from run *C6*. Since the convection produces a vertical redistribution, the averaging renders this almost invisible - as it does vertical advection and turbulent diffusion - and the effects of convection on the chemistry should be more apparent. However, as time passes, there may subsequently be a difference in horizontal location of the pollutants if the wind speed and direction varies with height. Therefore care should be taken when comparing the vertically-integrated distributions between numerical runs.

Differences between the results of runs *C6* and *C7* are cumulative, and therefore should be more visible in the later stages of the integrations. After 12 hours, convective transport decreases [NO_x] by half over north-east England, but elsewhere concentrations are similar - compare Figure 7(a) with Figure 4(b). Some NO_x at the plume leading edge has spread northwards in run *C7*; this component of the plume has been raised by the convection to higher levels, where the wind has a more northward component. Figure 7(b) and Figure 5(b) show [*N(v)*] at 1200h. The convective transport produces a similar effect, namely the horizontal spreading of the *N(v)* plume. At this time there is little indication from these figures of a change in the relative amounts of NO_x and *N(v)* anywhere, as would be expected if there were a significant change in the overall transformation rate between runs *C6* and *C7*.

At 1800h, however, there are regions where the convection changes [NO_x] and [*N(v)*] in opposite directions. A comparison of Figure 4(c) with Figure 7(c) shows an increase in [NO_x] over eastern England. Comparing Figure 5(c) and Figure 7(d) shows a decrease in [*N(v)*] over the same region. Hence there is a definite effect of convection in locally reducing the oxidation rate from NO_x to *N(v)*. The main effect of the convection is still in redistributing NO_x and *N(v)* both vertically and horizontally, rather than in changing their relative proportions. Changes in the distribution of *N(v)* are important, as the oxidized nitrogen compounds have the potential to be scavenged and deposited at the surface in acidic precipitation. This is addressed next.

3.4 Run C8: Scavenging by grid-scale precipitation only

Only *N(v)* compounds are scavenged by precipitation in this model, hence *NO* and NO_2 concentrations are identical to those in run *C6*. The solubility of nitric oxide and nitrogen dioxide is neglected. In run *C8* there is no convective transport of pollutants. Figure 8 shows the domain totals of NO_x, NO_2, airborne *N(v)* and deposited *N(v)*. The NO_x and NO_2 curves are identical to those in Figure 2. The amount of *N(v)* removed increases gradually through the period of integration, with the most rapid scavenging rate between 0900h and 1200h, during which time the amount of *N(v)* remaining airborne decreases. Roughly 40% of the *N(v)* is removed by

gridscale, stratiform rain in the 18 hour integration, from all levels in the *N(v)* plume.

Scavenging and deposition occur where dynamic rainfall coincides with the pollutant plume. Six-hourly deposition totals are shown in Figure 9 for run *C8* due to stratiform rain. Deposition to the sea surface is included. Rainfall over Northern Ireland and the Irish Sea washes out *N(v)* in the first six hours (Figure 9(a)). In the following six hours, the *N(v)* plume advances over England, where it encounters orographically forced rain over the Pennines and Lake District hills, depositing material rapidly over the land. This period includes the steepest section of the dot-dashed curve in Figure 8. Later, the *N(v)* plume reaches the North Sea, where there is widespread stratiform and convective rainfall. The stratiform rain in this run thus washes out *N(v)* mainly to the sea surface in the last six hours (Figure 9(c)). There is little deposition to the land surface in this period, as the portion of the *N(v)* plume over the land is south of its position in the middle six hours, over locations where there is no rainfall.

3.5 Run C9: Scavenging by convective and dynamic rain

Run *C9* adds the convective parametrization for pollutants to run *C8*, which includes scavenging. Run *C9* is also equivalent to run *C7* with scavenging, hence results for *NO* and NO_2 for run *C9* are the same as those for run *C7*. *N(v)* is removed by convective and dynamic rain in this run. Convective rain scavenges *N(v)* from different levels to dynamic rain, leaving a different vertical distribution of airborne *N(v)*, and material is deposited at different surface locations.

More *N(v)* is removed in total in run *C9* than in run *C8*. Convective rain removes less than dynamic rain in run *C9*, as the latter is more widespread. This is summarized in Table 2 for domain totals of *N(v)* at 1600h.

Run	Total *N(v)*	Airborne *N(v)*	Deposited (dynamic)	Deposited (convective)
C8	12.2	7.0 (58%)	5.2 (42%)	0

C9	11.5	5.2 (45%)	3.7 (32%)	2.6 (23%)

Table 2: Domain N(v) totals. Units are multiples of 1000 kg(N), with the percentage of the total N(v) in brackets.

As shown in previous sections, the production rate of *N(v)* is decreased by convective effects, hence the slightly different totals of *N(v)* in Table 2. The percentage of *N(v)* remaining airborne is also decreased by convective effects, and not only is the deposition location likely to be altered, but *N(v)* is deposited over a sub-gridscale area, and so will be more concentrated at the surface. The deposition patterns resulting from removal by stratiform precipitation are qualitatively similar in run *C9* to those shown in Figure 9, except the amounts of *N(v)* deposited are generally less in this run, as less airborne *N(v)* is available for removal by stratiform rain if it has been previously scavenged by convective rain.

Scavenging and deposition due to convective rain produce quite different surface patterns from those due to dynamic rain, as shown in Figure 10. In the first six hours of integration, there is little convection; it is still night time and the sea surface and boundary layer are still cool. Hence deposition amounts are small during this period (Figure 10(a)). In the next six hours, convection becomes active over the Irish Sea as the surface warms, and, since the *N(v)* plume extends across this region, there is significant deposition there (Figure 10(b)). This contrasts with deposition due to dynamic rain which occurs over land, as in Figure 9(b). In the final six hours, the convection penetrates inland through the so-called "Cheshire gap". Significant amounts of *N(v)* are thus deposited in this region (Figure 10(c)). The plume itself extends as far as the North Sea by this time, and there is deposition there, from both convective and dynamic rainfall.

Comparing the total amount removed with that deposited at the land surface shows that in the full 18-hour integration, 18% more *N(v)* is removed in run *C9* than in run *C8*, but the increase in deposition to the land is 2%. The extra removal mechanism included in run *C9* occurs in this case mainly over the sea. It is possible that for other emission scenarios, convective effects on the chemical species may make the land surface less polluted. What is

demonstrated in this work is the necessity to incorporate the effects of convection on transport and removal into the mesoscale model. Also, although convection is in this case relatively sparse, chemical reactions, in terms of the oxidation rates and the chemical lifetimes of the emitted pollutants, are still found to be affected by convective processes. Scavenging and deposition patterns are greatly affected by convection.

4 Discussion

The results described in the previous section demonstrate the effect of cumulus convection on rates of chemical transformations and precipitation scavenging. The convection is sub-gridscale, with tracer transport parametrized as described by Gimson (1997). A simple chemical model is employed, involving the oxidized nitrogen species from the EMEP model (Sandnes, 1993), simplified further to a one-way sequence of transformations, from NO_x emissions into the atmosphere, through oxidation to *N(v)* compounds, to scavenging and deposition of *N(v)*. The main findings may be summarized as follows:-

- The total amount of NO_x in the model domain is affected little by convection.
- At some locations over land, the column-averaged rate of reaction from NO_x to *N(v)* is reduced by convective effects, as contaminants rise to levels of lower temperature and background-species concentration.
- A complex interaction exists between convective transport, turbulent diffusion, and chemistry, where at different times and at different levels, different processes may be important.
- Convective rain is an efficient scavenger of *N(v)* - despite the small convective cloud cover - and changes qualitatively the location of deposition to the surface.
- Contaminants are deposited by sub-gridscale convection over only a fraction of a mesoscale grid-square, producing higher local surface concentrations.

With reference to the last point, a convective cloud covering an area one-tenth of the grid area, passing over a grid square from SW to NE, rains on only one-third of that square. Therefore, since Figure 10 shows the grid-averaged values of deposition, actual deposition amounts could locally be up to three times those shown.

Although the effects of convection on the domain-averaged chemical lifetimes are not great in the mesoscale model integrations, it must be pointed out that these effects should accumulate over periods of days, as typical oxidation time-scales given in Appendix A are of the order of a few hours. Locally, the effects are more significant over shorter times. For more rapid chemical reactions, the interaction between chemistry and convection will be more complex, as time-scales associated with each process will be more similar. This is for future investigation.

Some discussion of the applicability of the EMEP scheme to mesoscale modelling is required. The original scheme operates on a 150 km grid and is specific to the atmospheric boundary layer. Reaction rates in this paper have been modified to account for variation with height of the concentrations of background reactants O_3 and OH from Isaksen and Hov (1987). The removal parametrization has been modified for use in this paper, by letting the scavenging ratio apply at all levels and letting the height scales h_j be the overlap depth of cloud and $N(v)$ plume; in the EMEP scheme the height scale is the boundary layer depth. The only water variable used in the scavenging routine is the precipitation rate, and the solution and oxidation of species such as NO_2 in cloud water are not modelled. Oxidation processes may be more rapid in the aqueous phase than in the gas phase. There are many cloud chemistry models available, in which the solution and oxidation of airborne species in cloud and rain are described, for example Hill *et al.* (1986), Carmichael *et al.* (1986), Tremblay and Leighton (1986), Chang *et al.* (1987), Iribarne and Cho (1989), Berge (1993) and Wang and Chang (1993a). These are incorporated into regional scale or mesoscale meteorological models and require realistic representations of water vapour and cloud water/ice for realistic chemical balances between airborne and dissolved species. An examination of the realism of these micro-physical

quantities in the mesoscale model is required, particularly in the convection parametrization, before such chemical models should be implemented. It is known that the application of different convective parametrizations (to the same chemistry) yield differing concentrations of the chemical species (see, for example, Mölders and Laube, 1994).

However, this is highly worthwhile pursuing. A natural extension of the chemical scheme used here would include the prognosis, rather than the pre-specification, of ozone and the hydroxyl radical. These are important oxidant species for tropospheric trace gases, and their reactions involve the dissociation of water molecules in the vapour phase. The extended chemical scheme, and a more realistic convection scheme could then be reliably coupled - including the effects of the presence of cloud on photolysis rates - to model ozone and its precursors, in the boundary layer and free troposphere, at mesoscale and longer ranges. Ozone is an indicator of photochemical activity and urban pollution in the lower troposphere, and a greenhouse gas in the upper troposphere. The modelling and prediction of the interactions between photo-chemistry and cumulus convection are therefore important avenues for present and future research.

5 Acknowledgements

This work has benefited greatly from discussions with Prof. Alan Thorpe and Dr. Deb Fish of the Department of Meteorology, University of Reading. The research was funded by NERC, grant number GR3/8419.

6 Appendix A - Reaction rates of oxides of nitrogen

This Appendix describes the nitrogen chemistry used in the model. The equations describing the chemical kinetics are as follows:

$$\frac{d[NO_2]}{dt} = 0.05 \times 0.96Q - \frac{[NO_2]}{\tau_4} + \frac{[NO]}{\tau_5} - \frac{0.001 \times [NO_2]}{1.25} - \frac{[NO_2]}{\tau_8} - \frac{[NO_2]}{\tau_{12}}$$

Equation 3

$$\frac{d[NO]}{dt} = 0.95 \times Q + \frac{[NO_2]}{\tau_4} - \frac{[NO]}{\tau_5}$$

Equation 4

$$\frac{d[HNO_3]}{dt} = \frac{[NO_2]}{\tau_8} - \frac{[HNO_3]}{\tau_d} - \sigma$$

Equation 5

$$\frac{d[NO_3]}{dt} = \frac{[NO_2]}{\tau_{12}} - \frac{[NO_3]}{\tau_d} - \sigma$$

Equation 6

NO_x is emitted at a rate Q (kg(N) m^{-3} s^{-1}), consisting of 95% *NO* and 5% NO_2. 4% of the NO_2 is deposited at the source, hence

$$S_e = (1 - 0.05 \times 0.04)Q.$$

NO_2 converts to *NO* via photolysis, such that

$$NO_2 + h\nu \rightarrow NO + O^*$$

Equation 7

at a rate

$$\frac{1}{\tau_4} = 0.01 \exp(-0.39 \sec(\zeta)),$$

where sec(ζ) is the secant of the solar zenith angle. At night the rate is zero. *NO* converts to NO_2 through the following reaction:

$$NO + O_3 \rightarrow NO + O_2$$

Equation 8

The excited oxygen atom, denoted O^* in Equation 7, quickly reacts with oxygen gas to form the ozone for this reaction. Here, ozone is pre-specified as a height-varying distribution, decreasing linearly from 1.75×10^{12} molecules cm^{-3} at the surface to 1.0×10^{12} molecules cm^{-3} at $\eta = 4$ km, constant to 12 km and increasing again above that height (similar to Isaksen and Hov (1987)). Then

$$\frac{1}{\tau_5} = 2.1 \times 10^{-12} \times [O_3] \times \exp\left(\frac{-1450}{T}\right)$$

gives the rate of conversion from *NO* to NO_2 in Equation 8. *T* is the temperature in Kelvins. τ_4 and τ_5 are relatively short time-scales, both less than about 5 minutes, hence *NO* and NO_2 may be considered in equilibrium, with

$$\frac{[NO_2]}{\tau_4} = \frac{[NO]}{\tau_5}.$$

Since $[NO_x] = [NO] + [NO_2]$, then

$$[NO_2] = \frac{\tau_4}{\tau_4 + \tau_5}[NO_x],$$

and NO_x will be the dependent variable used in the model. NO_2 is subject to dry deposition over land, removed from the lowest model level (height 1.25 m) with a deposition velocity 0.001 m s^{-1}.
NO_2 reacts with the hydroxyl radical to produce nitric acid:

$$NO_2 + OH \rightarrow HNO_3.$$

Equation 9

[*OH*] varies diurnally and seasonally, so Berge's (1993) formulation is used for autumn, in the presence of anthropogenic emissions, with the altitude variation of Isaksen and Hov (1987) superposed. Thus

$$[OH] = 1.5 \times 10^6 (1 + 0.3\cos(\zeta)) f_r ,$$

where cos(ζ) is the cosine of the solar zenith angle. f_r varies from 1.2 to 0.4 between the surface and η = 2.5 km , is constant up to 12 km , and decreases again higher up. Then

$$\frac{1}{\tau_8} = [OH] \times 1.1 \times 10^{-11}$$

gives the rate of the reaction in Equation 9. *OH* is produced by photolysis of ozone, via reaction with water vapour, which occurs during the day. Hence this reaction of NO_2 is not allowed to occur at night.

At night, NO_2 reacts with ozone, leading to production of particulate nitrate, at a rate

$$\frac{1}{\tau_{12}} = 2[O_3] \times 1.2 \times 10^{-13} \exp\left(\frac{-2450}{T}\right).$$

This represents a composite of the following series of reactions:

$$NO_2 + O_3 \rightarrow NO_3 + O_2$$
$$NO_3 + NO_2 \leftrightarrow N_2O_5$$
$$N_2O_5 + H_2O \rightarrow 2NO^-_{3(s)} + 2H^+ ,$$

with the first of the series being the rate limiting step. During the day, the nitrate radical, NO_3, photo-dissociates to *NO* and NO_2 and this reaction does not proceed to nitrate particles.

The reaction scheme considered in this work contains a subset of the reactions that NO_x compounds are subject to. Others, such as reaction with

the peroxyacetyl radical to form peroxyacetyl nitrate (PAN), and the thermal decomposition of PAN which results in NO_2 are neglected here.

Assuming that HNO_3 and NO_3^- are not subsequently reduced* , and that they are removed at the same rate, they may be combined into one variable, called $N(v)$, such that $[N(v)] = [HNO_3] + [NO_3^-]$. Then the gas-to-particle and particle-to-gas reactions between the two species may be ignored. (The EMEP scheme assumes the gas-to-particle rate is double the reverse reaction rate). Reaction of nitric acid and ammonia to produce ammonium nitrate is neglected in this scheme.

$N(v)$ is subject to dry deposition over both land and sea, removed from the lowest model level with a deposition velocity 0.002 m s^{-1}.

Adding Equation 3 and Equation 4 leads to

$$\frac{d[NO_x]}{dt} = S_e - \frac{\tau_4}{\tau_4 + \tau_5}\left(\frac{1}{\tau_8} + \frac{1}{\tau_{12}} + \frac{0.001}{1.25}\right)[NO_x].$$

Equation 10

Adding Equation 5 and Equation 6 leads to

$$\frac{d[N(v)]}{dt} = \frac{\tau_4}{\tau_4 + \tau_5}\left(\frac{1}{\tau_8} + \frac{1}{\tau_{12}}\right)[NO_x] - \frac{0.002}{1.25}[N(v)].$$

Equation 11

From Equation 10 and Equation 11 the definitions of τ_a, τ_b and τ_d follow in section 2. Source and sink rates derived here are applied to both in-cloud and environment quantities.

7 Appendix B - Scavenging rates

It is known that NO and NO_2 gases are soluble in rain water and will further oxidize to nitrate ions. This is secondary to the solution of already oxidized nitrate species. Introducing the rainborne component $[N(v)]_r$ (in kg(N) m^{-3}_{rain})

* Nitric acid is photolysed, but with a typical time scale of 20 days; it is neglected here.

of $[N(v)]_1$, and assuming the in-cloud scavenging from the airborne component to the cloud rainwater component is on the time-scale τ_1, the following is obtained (ignoring other processes):

$$\frac{\partial [N(v)]_1}{\partial t} = -\frac{[N(v)]_1}{\tau_1} = -\sigma_1$$

and

$$\frac{\partial}{\partial t}\left(R[N(v)]_r\right) = \frac{[N(v)]_1}{\tau_1} + \frac{\partial}{\partial \eta}\left(R\omega[N(v)]_r\right),$$

Equation 12

where R is the volume fraction of rainwater (in $m^3_{rain}\ m^{-3}_{air}$) and ω is the rainfall speed (positive downwards). In Equation 12 a term for the flux of $N(v)$ in falling rain is included. To incorporate these processes into the model, some simplifying assumptions must be made; (i) a steady-state balance between scavenging and flux to the surface in rain exists ($\partial R[N(v)]_r/\partial t = 0$) and (ii) the scavenging is also in equilibrium and a constant scavenging ratio applies, whence $[N(v)]_r = \Lambda_v[N(v)]_1$. Also, it can be seen that $R\omega = p/\rho_w$, where p is the mean precipitation rate over the convective updraught and ρ_w is the density of water. Then Equation 12 becomes

$$\frac{[N(v)]_1}{\tau_1} = -\frac{\partial}{\partial \eta}\left(\frac{p\Lambda_v}{\rho_w}[N(v)]_1\right).$$

Equation 13

Further simplification involves the definition of a height scale h_1, giving

$$\frac{\partial}{\partial \eta}\left(\frac{p\Lambda_v}{\rho_w}[N(v)]_1\right) = -\frac{p\Lambda_v[N(v)]_1}{\rho_w h_1}.$$

Equation 14

Equation 14 is not itself an approximation to Equation 13, except that the height scale is not height-dependent. In such a case it is possible to integrate from the surface to the top of the domain ($\eta = H_{TOP}$), leading to

$$h_1 = \frac{\int_0^{H_{TOP}} p[N(v)]_1 d\eta}{\left(p[N(v)]_1\right)_{\eta=0}}.$$

To avoid dividing by zero this is modified to

$$h_1 = \frac{\int_0^{H_{TOP}} p[N(v)]_1 d\eta}{p_{\eta=0} \times \max\left([N(v)]_1\right)}.$$

Equation 15

where the maximum is over the depth of the convective column. The scale height has been introduced purely to enable expression in terms of integrals rather than differentials. There is little physical justification for it, except that h_1 is effectively an overlap depth of plume and rain-shaft. A knowledge of the vertical structure of the precipitation is required, which is based on the cloud-resolving model results in Gimson (1997). The convective precipitation rate increases from its surface value to twice this value at the cloud middle level, then decreases to zero at the cloud top level.

With h_1 calculated from Equation 15, Equation 13 and Equation 14 are combined to give

$$\frac{1}{\tau_1} = \frac{p\Lambda_v}{\rho_w h_1},$$

as used in the main text. This is also the form used by the EMEP model Sandnes (1993). τ_2, τ_3, h_2 and h_3 are calculated analogously, using suitable values for the rainfall rates, defined in the main body of the paper.

8 References

Berge, E., 1993: Coupling of wet scavenging of sulphur to clouds in a numerical weather prediction model. *Tellus* **43B**, 1-22.

Berkowitz, C.M., Easter, R.C. and Scott, B.C., 1989: Theory and results from a quasi-steady-state precipitation-scavenging model. *Atmos. Environ.* **23**, 1555-1571.

Carmichael, G.R., Peters, L.K. and Kitada, T., 1986: A second generation model for regional-scale transport/chemistry/deposition. *Atmos. Environ.* **20**, 173-188.

Carmichael, G.R., Peters, L.K. and Saylor, R.D., 1991: The STEM-II regional-scale acid deposition and photochemical oxidant model - I. An overview of model development and applications. *Atmos. Environ.* **25A**, 2077-2090.

Chang, J.S., Brost, R.A., Isaksen, I.S.A., Madronich, S., Middleton, P., Stockwell, W.R. and Walcek, C.J., 1987: A three-dimensional eulerian acid deposition model: Physical concepts and formulation. *J. Geophys. Res.* **92**, 14681-14700.

Cho, H.-R., Niewiadomski, M., Iribarne, J.V. and Melo, O., 1989: A model of the effect of cumulus clouds on the redistribution and transformation of pollutants. *J. Geophys. Res.* **94D**, 12895-12910.

Derwent, R.G., 1990: Evaluation of a number of chemical mechanisms for their application in models describing the formation of photochemical ozone in Europe. *Atmos. Environ.* **24A**, 2615-2624.

Derwent, R.G., 1993: Evaluation of the chemical mechanism employed in the EMEP photochemical oxidant model. *Atmos. Environ.* **27A**, 277-279.

Elliott, S., Kao, C.-Y.J., Gifford, F., Barr, S., Shen, M., Turco, R.P., and Jacobson, M., 1996: Free tropospheric ozone production after deep convection of dispersing tropical urban plumes. *Atmos. Environ.* **30**, 4263-4274.

Gimson, N.R., 1994: Dispersion and removal of pollutants during the passage of an atmospheric frontal system. *Q. J. R. Meteorol. Soc.* **120**, 139-160.

Gimson, N.R., 1997: Pollution transport by convective clouds in a mesoscale model. *Q. J. R. Meteorol. Soc.* **123**, 1805-1828.

Golding, B.W., 1990: The Meteorological Office mesoscale model. *Meteorol. Mag.*, **119**, 81-96.

Hill, T.A., Choularton, T.W., and Penkett, S.A., 1986: A model of sulphate production in a cap cloud and subsequent turbulent deposition onto the hill surface. *Atmos. Environ.* **20**, 1763-1771.

Hong, M.-S., and Carmichael, G.R., 1986: Examination of a subgrid-scale parametrization for the transport of pollutants in a nonprecipitating cumulus cloud ensemble. *Atmos. Environ.* **20**, 2205-2217.

Hov, Ø., and Flatøy, F., 1997: Convective redistribution of ozone and oxides of nitrogen in the troposphere over Europe in summer and fall. *J. Atmos. Chem.* **28**, 319-337.

Iribarne, J.V. and Cho, H.-R., 1989: Models of cloud chemistry. *Tellus* **41B**, 2-23.

Isaksen, I.S.A. and Hov, Ø., 1987: Calculation of trends in the tropospheric concentrations of O_3, *OH*, *CO* and NO_x. *Tellus* **39B**, 271-285.

Karamchandani, P. and Venkatram, A., 1992: The role of non-precipitating clouds in producing ambient sulfate during summer: results from simulations with the acid deposition and oxidant model (ADOM). *Atmos. Environ.* **26A**, 1041-1052.

Leighton, H.G., Lauzon,.L., and Leaitch, W.R., 1996: Evaluation of a three-dimensional cloud chemistry model. *Atmos. Environ.* **30**, 3651-3665.

Lelieveld, J., and Crutzen, P.J., 1994: Role of deep cloud convection in the ozone budget of the troposphere. *Science* **264**, 1759-1761.

Lin, X., Ridley, B.A., Walega, J., Hübler, G.F., McKeen, S.A., Hsie, E.-Y., Trainer, M., Fehsenfeld, F.C., and Liu, S.C., 1994: Parameterization of subgrid scale convective cloud transport in a mesoscale regional chemistry model. *J. Geophys. Res.* **99D**, 25615-25630.

Mölders, N., and Laube, M., 1994: A numerical study on the influence of different cloud treatment in a chemical transport model on gas phase distribution. *Atmos. Research* **32**, 249-272.

Niewiadomski, M., 1989: Sulphur dioxide and sulphate in a three-dimensional field of convective clouds: numerical simulation. *Atmos. Environ.* **23**, 477-487.

Pickering, K.E., Thompson, A.M., Scala, J.R., Tao, W.-K., Dickerson, R.R., and Simpson, J., 1992: Free tropospheric ozone production following entrainment of urban plumes into deep convection. *J. Geophys. Res.* **97D**, 17985-18000.

Ridley, B.A., Walega, J., Dye, J.E., and Grahek, F.E., 1994: Distributions of NO, NO_x, NO_y and O_3 to 12 km altitude during the summer monsoon season over New Mexico. *J. Geophys. Res.* **99D**, 25519-25534.

Sandnes, H., 1993: Calculated budgets for airborne acidifying components in Europe, 1985, 1987, 1988, 1989, 1990, 1991 and 1992. *Technical report 109*, The Norwegian Meteorological Institute.

Thompson, A.M., Pickering, K.E., Dickerson, R.R., Ellis, W.G., Jacob, D.J., Scala, J.R., Tao, W.-K., McNamara, D.P., and Simpson, J, 1994: Convective transport over the central United States and its role in regional CO and ozone budgets. *J. Geophys. Res.* **99D**, 18703-18711.

Tremblay, A., 1987: Cumulus cloud transport, scavenging and chemistry: observations and simulations. *Atmos. Environ.* **21**, 2345-2364.

Tremblay, A. and Leighton, H., 1986: A three-dimensional cloud chemistry model. *J. Clim. Appl. Meteorol.* **25**, 652-671.

Walcek, C.J. and Taylor, G.R., 1986: A theoretical method for computing vertical distributions of acidity and sulphate production within cumulus clouds. *J. Atmos. Sci.* **43**, 339-355.

Wang, C. and Chang, J.S., 1993a: A three-dimensional numerical model of cloud dynamics, microphysics, and chemistry. 1: Concepts and formulation. *J. Geophys. Res.* **98D**, 14827-14844.

Wang, C. and Chang, J.S., 1993b: A three-dimensional numerical model of cloud dynamics, microphysics, and chemistry. 3: Redistribution of pollutants. *J. Geophys. Res.* **98D**, 16787-16798.

Yuen, P.-F., Hegg, D.A., Larson, T.V., Barth, M.C., 1980: Parameterization of heterogeneous droplet chemistry for use in bulk cloud models. *J. Appl. Meteorol.* **35**, 679-689.

9 Figure captions.

Figure 1. Mesoscale-model output for midday, 23 October 1992. Convective cloud-top height (shaded), with contour levels 2, 3 and 4 km. Horizontal wind vectors (arrows) at 1.5 km, with maximum speed 25 m s^{-1}. Axes are marked in km.

Figure 2. Volume-total mass of the chemical species in run C6. NO_x (solid line), NO_2 (dotted line) and N(v) (dashed line).

Figure 3. Vertical profiles of horizontally-integrated species mass in run C6. Times are 6 hours (dot-dashed), 12 hours (dashed), 15 hours (dotted) and 18 hours (solid); (a) NO_x; (b) N(v).

Figure 4. Vertically-integrated mass of NO_x in run C6. Contour levels are 30, 60, 120 and 240 μg m^{-2}. Times are (a) 6 hours, (b) 12 hours and (c) 18 hours.

Figure 5. As figure 4, but for N(v) in run C6.

Figure 6. As figure 3, but for run C7.

Figure 7. Vertically-integrated mass of tracer species in run C7. (a) NO_x at 12 hours; (b) N(v) at 12 hours; (c) NO_x at 18 hours; (d) N(v) at 18 hours. Contour levels are as in figure 4.

Figure 8. . Volume-total mass of the chemical species in run C8. NO_x (solid line), NO_2 (dotted line), N(v) (dashed line) and wet deposition of N(v) (dot-dashed line).

Figure 9. Deposition of N(v) from scavenging by stratiform rain in run C8. Contour levels are 20, 60 and 180 μg m^{-2}. (a) Total deposited in the first 6 hours; (b) total deposition between 6 and 12 hours; (c) total deposited between 12 and 18 hours.

Figure 10. Deposition of N(v) from scavenging by convective rain in run C9. Contour levels are 10, 50 and 150 μg m^{-2}. (a) Total deposited in the first 6 hours; (b) total deposition between 6 and 12 hours; (c) total deposited between 12 and 18 hours.

Figure 1.

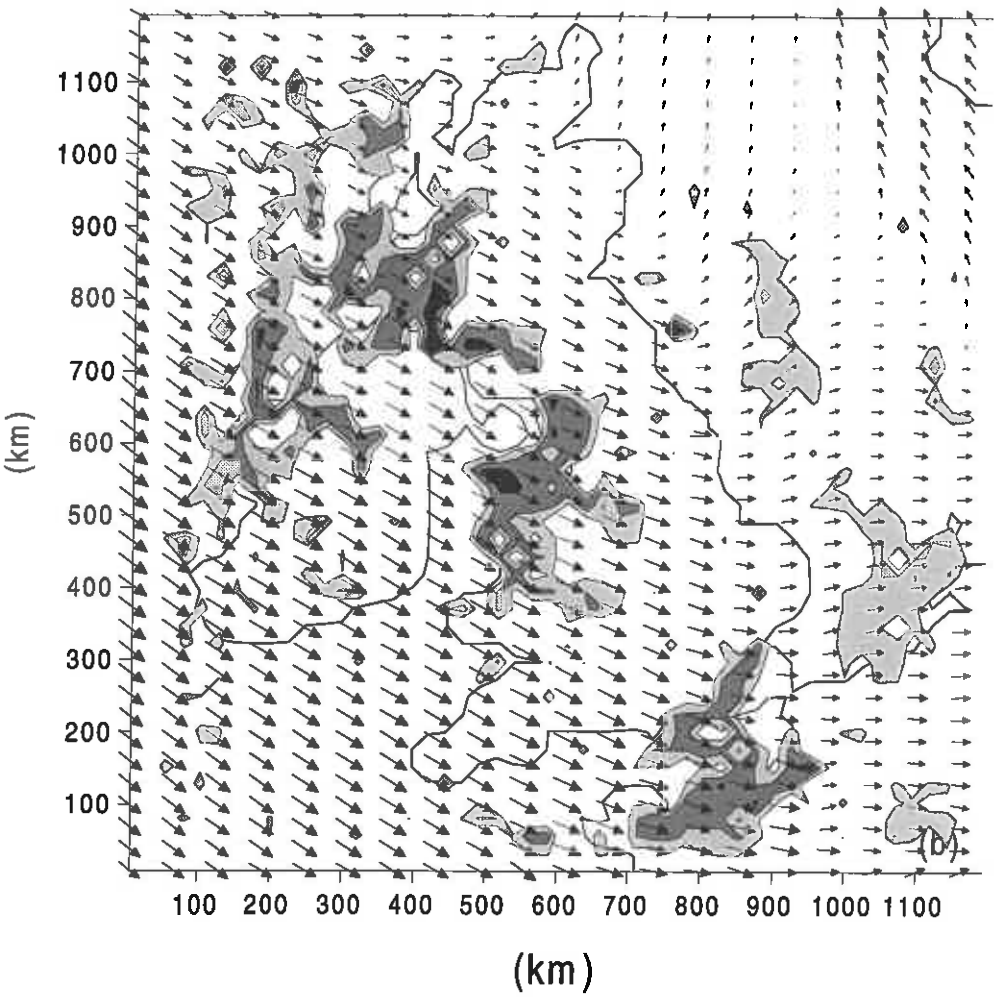

Figure 1. Mesoscale-model output for midday, 23 October 1992. Convective cloud-top height (shaded), with contour levels 2, 3 and 4 km. Horizontal wind vectors (arrows) at 1.5 km, with maximum speed 25 m s^{-1}. Axes are marked in km.

Figure 2.

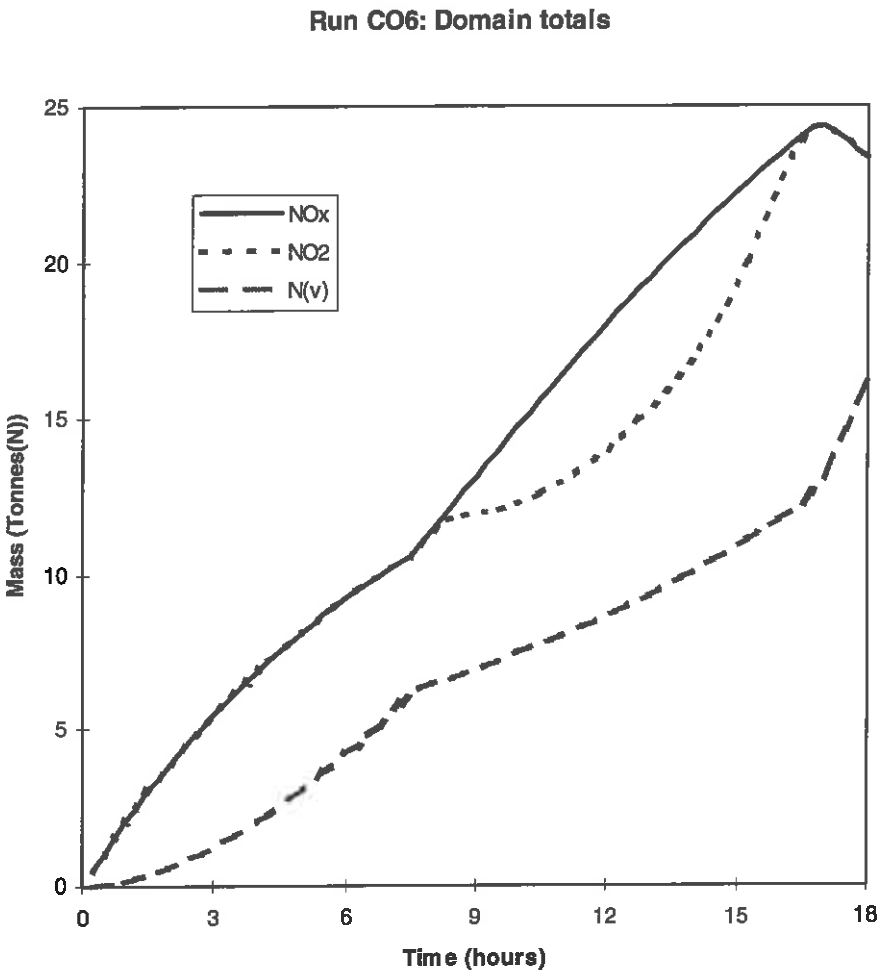

Figure 2. Volume-total mass of the chemical species in run C6. NO_x (solid line), NO_2 (dotted line) and N(v) (dashed line).

Figure 3.

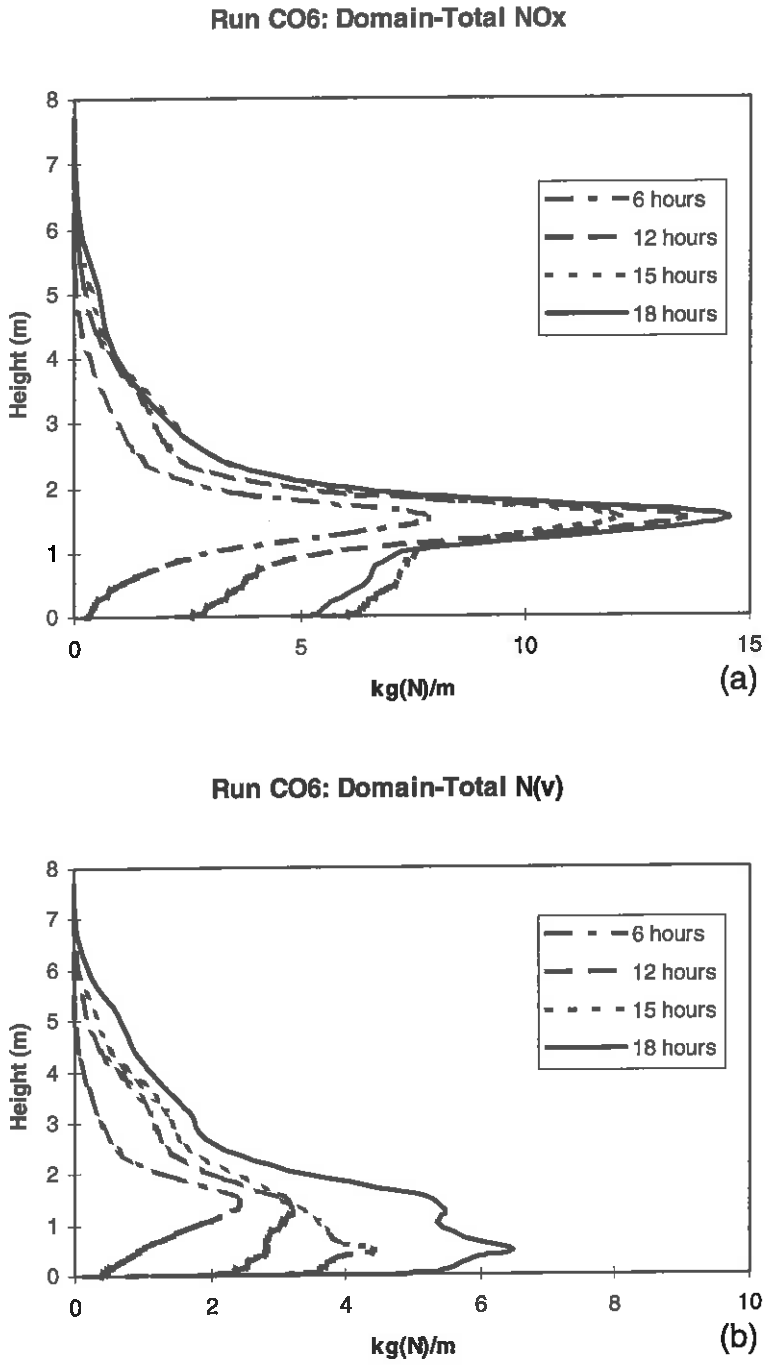

Figure 3. Vertical profiles of horizontally-integrated species mass in run C6. Times are 6 hours (dot-dashed), 12 hours (dashed), 15 hours (dotted) and 18 hours (solid); (a) NO_x; (b) N(v).

Figure 4.

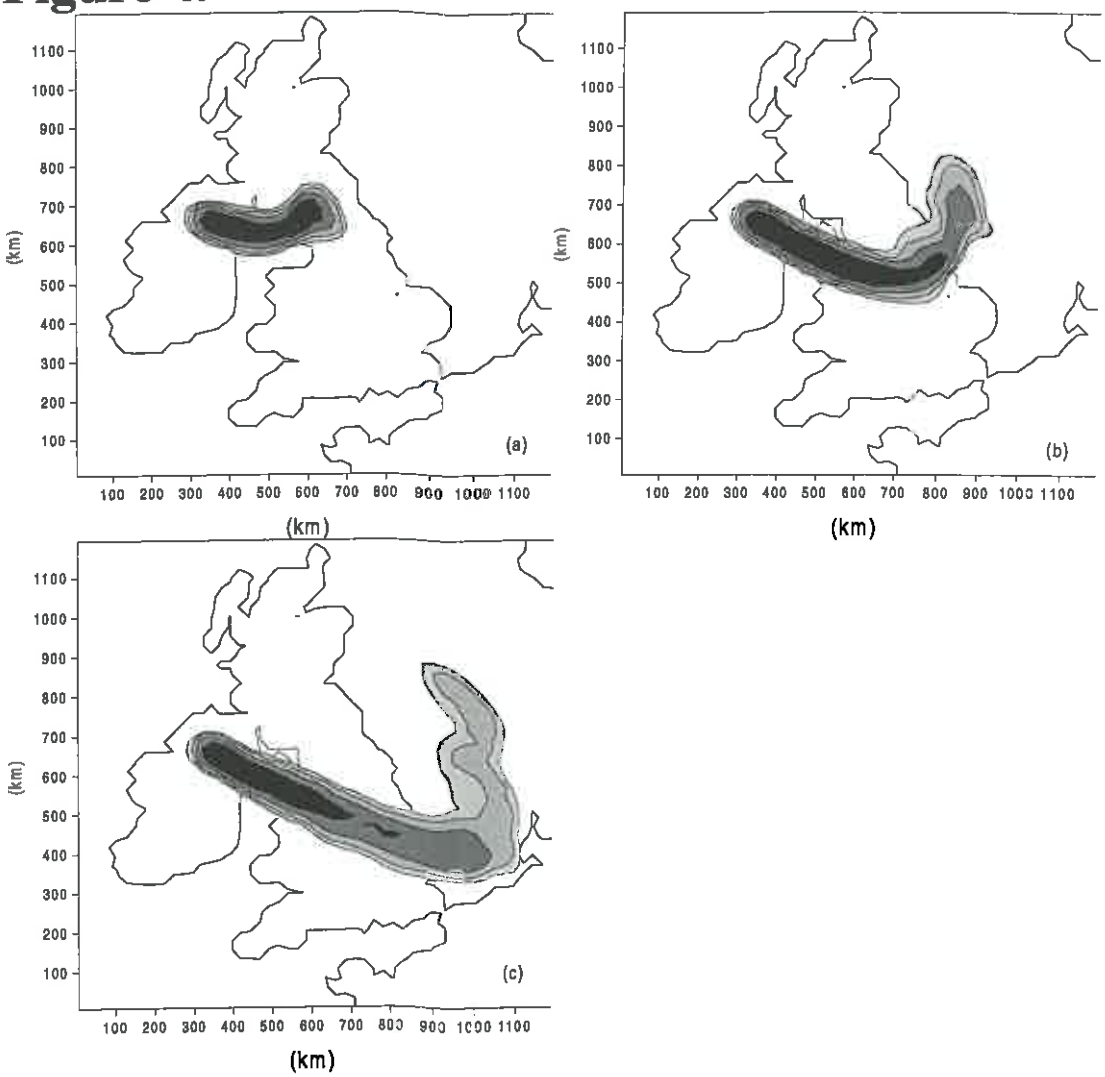

Figure 4. Vertically-integrated mass of NO_x in run C6. Contour levels are 30, 60, 120 and 240 μg m^{-2}. Times are (a) 6 hours, (b) 12 hours and (c) 18 hours.

Figure 5.

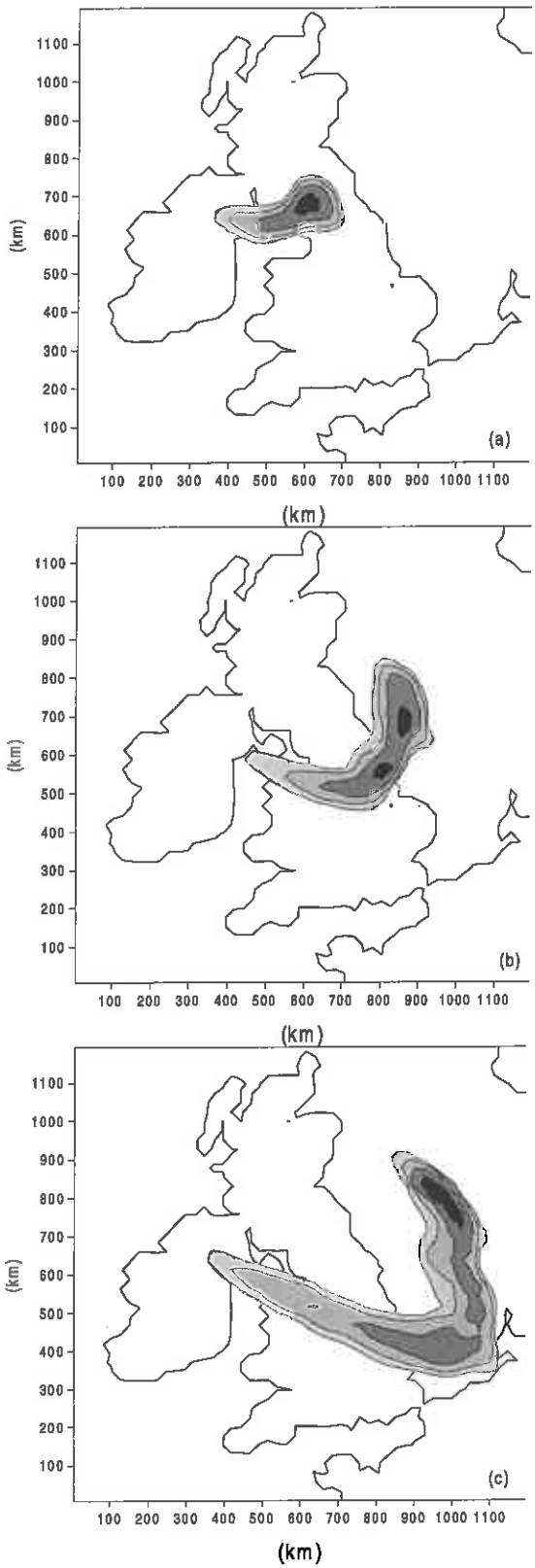

Figure 5. As figure 4, but for N(v) in run C6.

Figure 6.

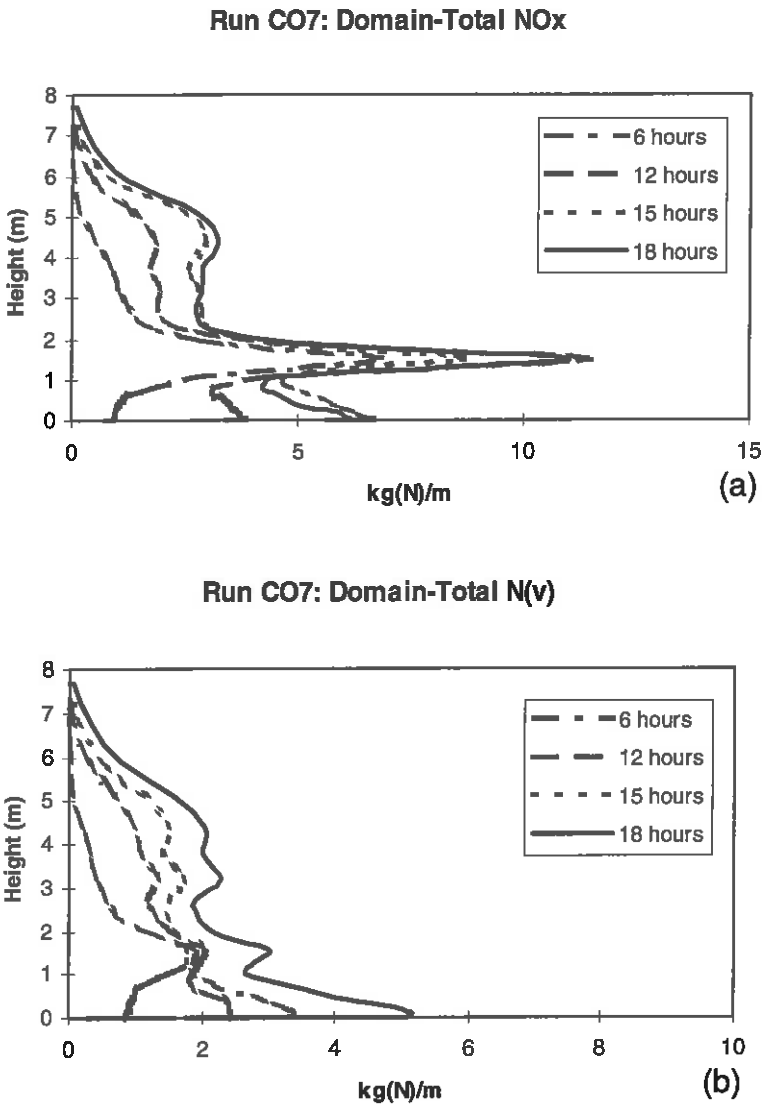

Figure 6. As figure 3, but for run C7.

Figure 7.

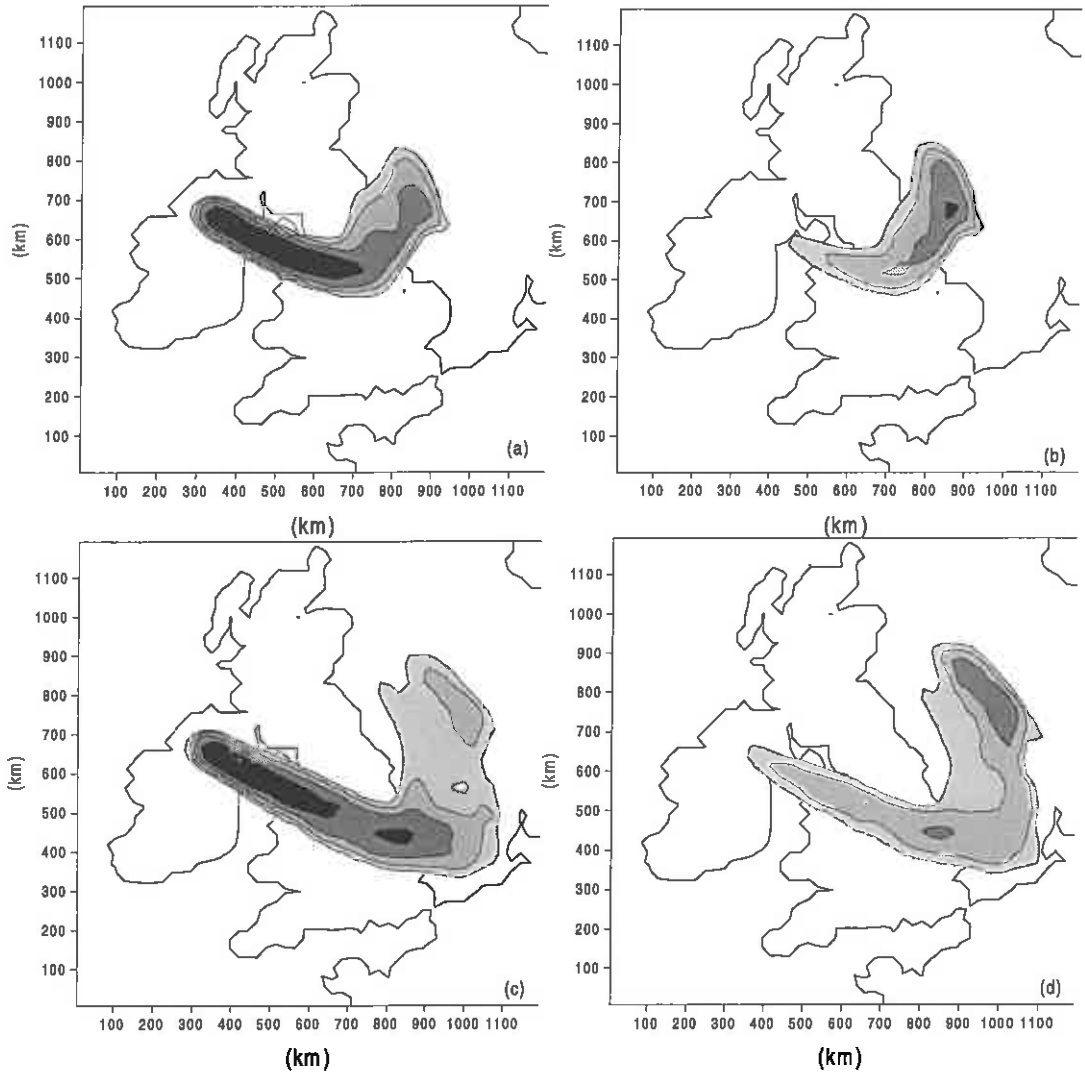

Figure 7. Vertically-integrated mass of tracer species in run C7. (a) NO_x at 12 hours; (b) N(v) at 12 hours; (c) NO_x at 18 hours; (d) N(v) at 18 hours. Contour levels are as in figure 4.

Figure 8.

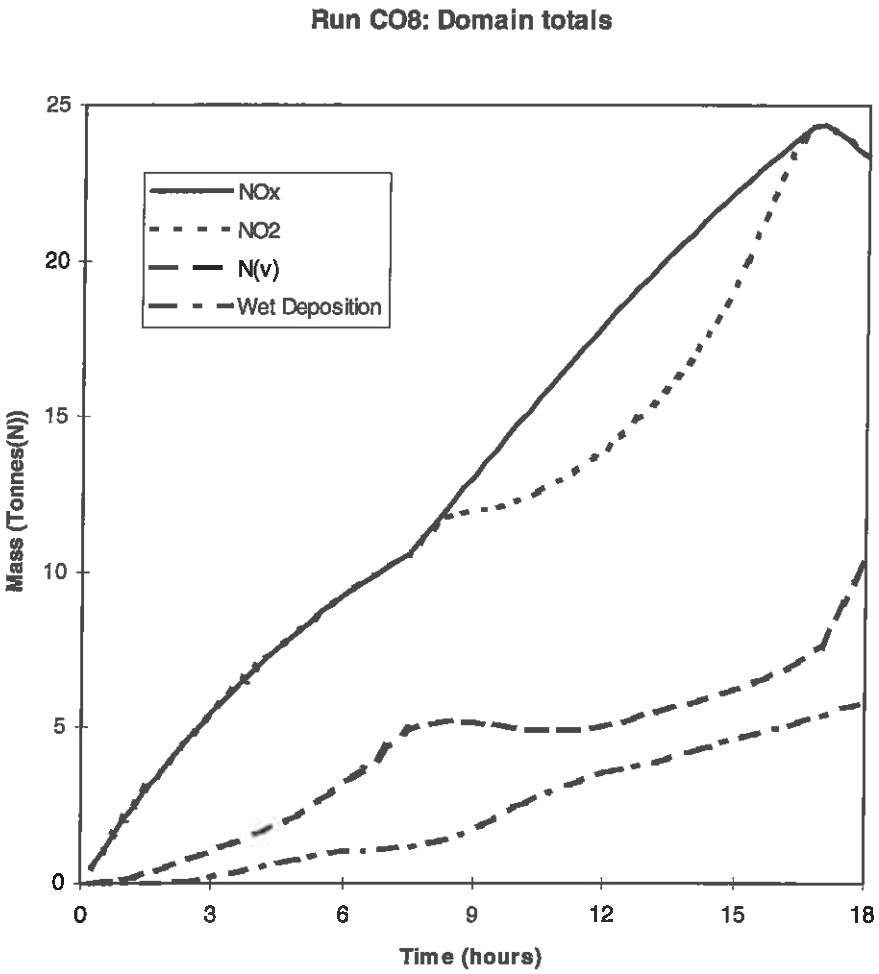

Figure 8. . Volume-total mass of the chemical species in run C8. NO_x (solid line), NO_2 (dotted line), N(v) (dashed line) and wet deposition of N(v) (dot-dashed line).

Figure 9.

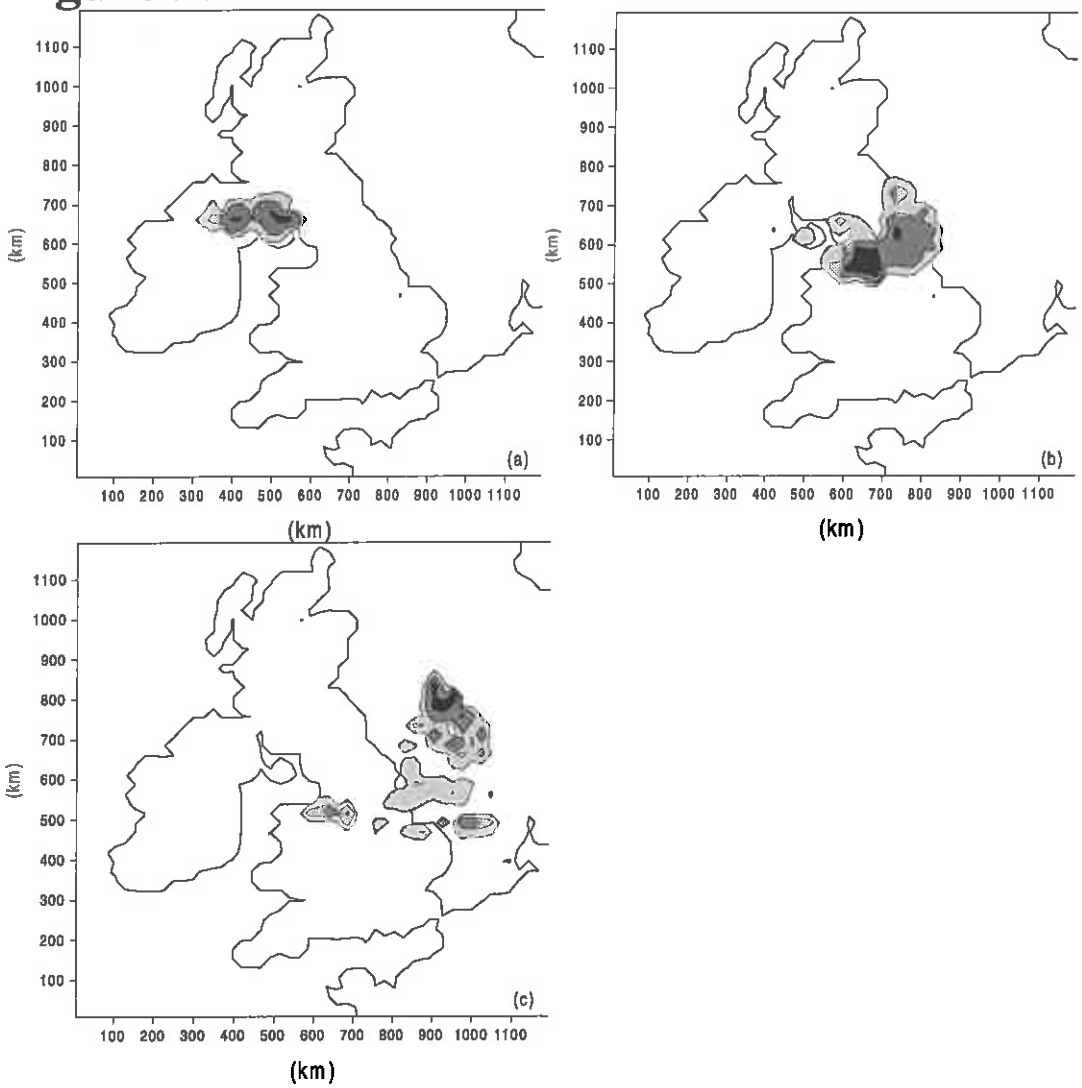

Figure 9. Deposition of N(v) from scavenging by stratiform rain in run C8. Contour levels are 20, 60 and 180 μg m^{-2}. (a) Total deposited in the first 6 hours; (b) total deposition between 6 and 12 hours; (c) total deposited between 12 and 18 hours.

Figure 10.

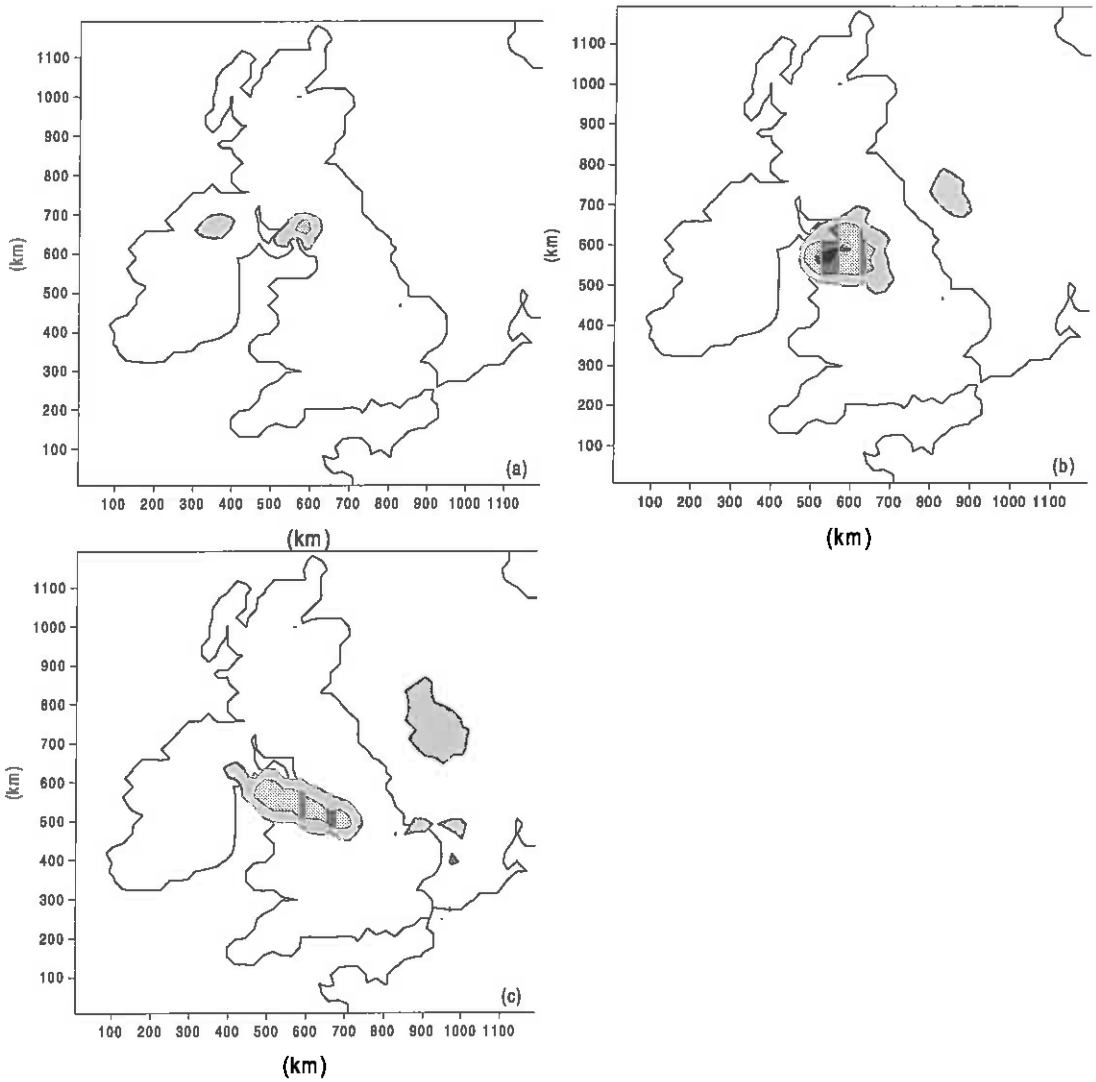

Figure 10. Deposition of N(v) from scavenging by convective rain in run C9. Contour levels are 10, 50 and 150 μg m^{-2}. (a) Total deposited in the first 6 hours; (b) total deposition between 6 and 12 hours; (c) total deposited between 12 and 18 hours.

CURRENT JCMM INTERNAL REPORTS

This series of JCMM Internal Reports, initiated in 1993, contains unpublished reports and also versions of articles submitted for publication. The complete set of Internal Reports is available from the National Meteorological Library on loan, if required.

1. **Research strategy and programme**
   K A Browning et al
   January 1993

2. **The GEWEX Cloud System Study (GCSS)**
   GEWEX Cloud System Science Team
   January 1993

3. **Evolution of a mesoscale upper tropospheric vorticity maximum and comma cloud from a cloud-free two dimensional potential vorticity anomaly**
   K A Browning
   January 1993

4. **The global energy and water cycle**
   K A Browning
   July 1993

5. **Structure of a midlatitude cyclone before occlusion**
   K A Browning and N Roberts
   July 1993

6. **Developments in systems and tools for weather forecasting**
   K A Browning and G Szejwach
   July 1993

7. **Diagnostic study of a narrow cold frontal rainband and severe winds associated with a stratospheric intrusion**
   K A Browning and R Reynolds
   August 1993

8. **Survey of perceived priority issues in the parametrizations of cloud-related processes in GCMs**
   K A Browning
   September 1993

9. **The effect of rain on longwave radiation**
   I Dharssi
   September 1993

10. **Cloud microphysical processes - a description of the parametrization used in the large eddy model**
    H Swann
    October 1993

11. **An appreciation of the meteorological research of Ernst Kleinschmidt**
    A J Thorpe
    May 1992

12. **Potential vorticity of flow along the Alps**
    A J Thorpe, H Volkert and Dietrich Heimann
    August 1992

13. **The representation of fronts**
    A J Thorpe
    January 1993

14. **A parametrization scheme for symmetric instability: test for an idealised flow**
C S Chan and A J Thorpe
February 1993

15. **The Fronts 92 Experiment: a Quicklook Atlas**
Edited by T D Hewson
November 1993

16. **Frontal wave stability during moist deformation frontogenesis**
Part 1: Linear wave dynamics
C H Bishop and A J Thorpe
May 1993

17. **Frontal wave stability during moist deformation frontogenesis**
Part 2. The suppression of non-linear wave development
C H Bishop and A J Thorpe
May 1993

18. **Gravity waves in sheared ducts**
S Monserrat and A J Thorpe
October 1993

19. **Potential vorticity and the electrostatics analogy: quasi-geostrophic theory**
C Bishop and A J Thorpe
November 1993

20. **Recent advances in the measurement of precipitation by radar**
A J Illingworth
April 1993

21. **Micro-physique et givrage: cloud microphysics and aircraft icing**
A J Illingworth
May 1993

22. **Differential phase measurements of precipitation**
M Blackman and A J Illingworth
May 1993

23. **Estimation of effective radius of cloud particles from the radar reflectivity**
N I Fox and A J Illingworth
May 1993

24. **A simple method of Dopplerising a pulsed magnetron radar**
A Hua, A J Illingworth and J Eastment
November 1993

25. **Radiation and polar lows**
George C Craig
February 1994

26. **Collected preprints submitted to the International Symposium on the Life Cycles of Extratropical Cyclones; Bergen, Norway, 27 June - 1 July 1994**
April 1994

27. **Convective frontogenesis**
Douglas J Parker and Alan J Thorpe
April 1994

28. **Improved measurement of the ice water content in cirrus using a total water evaporator**
Philip R A Brown and Peter N Francis
April 1994

29. **Mesoscale effects of a dry intrusion within a vigorous cyclone**
K A Browning and B W Golding
April 1994

30. **GEWEX Cloud System Study, Science Plan**
May 1994

31. **Parametrization of momentum transport by convectively generated gravity waves**
R Kershaw
May 1994

32. **Mesoscale Modelling Newsletter No 5**
May 1994

33. **Observations of the mesoscale sub-structure in the cold air of a developing frontal cyclone**
K A Browning, S A Clough, C S A Davitt, N M Roberts and T D Hewson
May 1994

34. **Longwave radiative forcing of a simulated tropical squall line**
Imtiaz Dharssi
July 1994

35. **On the nature of the convective circulation at a kata-cold front**
K A Browning
September 1994

36. **Collective preprints of papers submitted to the COST-75 International Seminar on Advanced Weather Radar Systems, Brussels, 20-23 September 1994**
November 1994

37. **Use of satellite imagery to diagnose events leading to frontal thunderstorms: Parts I and II of a case study**
K A Browning and N M Roberts
November 1994

38. **The role of spaceborne millimetre-wave radar in the global monitoring of ice cloud**
P R A Brown, A J Illingworth, A J Heymsfield, G M McFarquhar, K A Browning and M Gosset
December 1994

39. **Potential vorticity inversion**
Michal Ziemianski
October 1994

40. **Theory of mature tropical cyclones; a comparison between Kleinschmidt (1951) and Emanuel (1986)**
Suzanne L Gray
December 1994

41. **Dispersion and removal of pollutants during the passage of an atmospheric frontal system**
N R Gimson
December 1994

42. **The role of snow sublimation in frontogenesis**
D J Parker and A J Thorpe
December 1994

43. **Potential vorticity and the electrostatics Analogy: Ertel-Rossby formulation**
A J Thorpe and C H Bishop
December 1994

44. **Mesoscale aspect of extratropical cyclones: an observational perspective**
K A Browning
January 1995

45. **A polar low outbreak: evolution and mesoscale structures**
T D Hewson, G C Craig and C Claud
February 1995

46. **Generation of near-surface gusts of deep convection**
K Nakamura and R Kershaw
April 1995

47. **Attribution concepts applied to the Omega Equation**
S A Clough, C S A Davitt and A J Thorpe
June 1995

48. **Parametrization of mixed-phase cloud and precipitation**
Susan P Ballard and M Gerard Hutchinson
June 1995

49. **Short-range forecasting of stratocumulus: initialization prediction**
Susan P Ballard, Simon D Jackson and B Macpherson
June 1995

50. **Contributions of the JCMM/Dept of Meteorology Radar Group to the 27th AMS Radar Meteorology Conference, Vail October 1995**
June 1995

51. **Cold pools in shear**
Douglas J Parker
September 1995

52. **High-resolution analysis of frontal fracture**
K A Browning, S P Ballard and C S A Davitt
September 1995

53. **The albedo of broken cloud fields: calculations using a modified two stream radiation code**
Imtiaz Dharssi and Roy Kershaw
October 1995

54. **Parametrization of momentum transport by convection. I: theory and cloud modelling results**
R Kershaw and D Gregory
November 1995

55. **Variation of frontal structure along a cold front**
K A Browning and N M Roberts
November 1995

56. **Secondary frontal waves**
Douglas Parker
December 1995

57. **Objective fronts**
T D Hewson
March 1996

58. **Mesoscale analysis of the activation of a cold front during cyclogenesis**
K A Browning, N M Roberts and A J Illingworth
June 1996

59. **Investigation of different representations of rain in a 1-d evaporation model**
H Swann
May 1996

60. **Parametrization of diabatic processes in the inversion of the omega-equation**
M Athanassiadou and A J Thorpe
June 1996

61. **The role of the environmental flow in the development of secondary frontal cyclones**
I A Renfrew, A J Thorpe and A Joly
June 1996

62. **Consequences of the geostrophic momentum approximation on barotropic instability**
S Malardel, A J Thorpe and A Joly
June 1996

63. **Contributions to the AMS/RMS Conference on Mesoscale Processes**
Reading, 9-13 September 1996

64. **Vorticity and potential vorticity in stratified flows interacting with an isolated obstacle**
Jorge A Gutiérrez and A J Thorpe
September 1996

65. **Triple point development: two case studies**
Douglas Parker
September 1996

66. **Radar observations of wind-shear splitting within evolving atmospheric Kelvin-Helmholtz billows**
D Chapman and K A Browning
April 1997

67. **Cold frontal structure derived from radar wind profilers**
K A Browning, D Jerrett, J Nash, T Oakley and N M Roberts
May 1997

68. **The dry intrusion and its effect on the frontal, cloud and precipitation structure of extratropical cyclones**
K A Browning - Text of invited special lecture at the Spring Conference
of the Meteorological Society of Japan, University of Tsukuba, 22 May 1997

69. **Met. Office Unified Model data, diagnostic graphics programs, and other observational data available from the JCMM through the aegis of the Universities Weather Research Network (UWERN).** (Plus supplement)
Peter Panagi and Ed Dicks
June 1997

70. **Contributions of the JCMM/Dept of Meteorology Radar Group to the 28th AMS Radar Meteorology Conference.** Austin, Texas
September 1997

71. **Sensitivity of short-range weather forecasts to local potential vorticity modifications**
Meral Demirtas and Alan Thorpe
July 1997

72. **Objective identification of frontal wave cyclones**
T D Hewson
August 1997

73. **Attribution and its application to mesoscale structure associated with tropopause folds**
A J Thorpe
September 1997

74. **The role of the environmental flow in the development of secondary frontal cyclones**
Ian A Renfrew, Alan J Thorpe and Craig H Bishop
September 1997

75. **Potential vorticity: a short history of its definitions and uses**
Alan J Thorpe and Hans Volkert
September 1997

76. **Superposing semi-geostrophic potential vorticity anomalies**
H R Birkett and A J Thorpe
September 1997

77. **Short period forecasting of catchment-scale precipitation.**
Part 1: the role of Numerical Weather Prediction
M A Pedder, M Haile and A J Thorpe
September 1997

78. **Verification of the tracking technique used in an experimental cloud motion wind inferring system**
Z Wang, K A Browning and G A Kelly
October 1997

79. **A preliminary study of Fourier series analysis for cloud tracking with GOES high temporal resolution images**
Z Wang
October 1997

80. **Analysis of an ex-tropical cyclone after reintensifying as a warm-core extratropical cyclone**
K A Browning, G Vaughan and P Panagi
November 1997

81. **A JCMM overview of FASTEX IOPs**
S A Clough, H W Lean, N M Roberts, H Birkett, J-P Chaboureau, R Dixon, M Griffiths, T D Hewson and A Montani
January 1998

82. **Programs for PV inversion and modification**
Meral Demirtas
December 1997

83. **Release of potential shearing instability in warm frontal zones**
D Chapman and K A Browning
February 1998

84. **The European Cloud-Resolving Modelling Programme (EUCREM)**
Summary Report from the coordinator
P W White
April 1998

85. **A frontal wave database**
T D Hewson
April 1998

86. **Layering observed in dropsoundings from IOP 1 of Fronts 92**
S A Clough
May 1998

87. **Use of wind-shear displays for Doppler radar data**
D Chapman and K A Browning
May 1998

88. **Radar estimates of rainfall rates at the ground in bright band and non-bright band events**
T J Smyth and A J Illingworth
June 1998

89. **Correction for attenuation of radar reflectivity using polarisation data**
T J Smyth and A J Illingworth
June 1998

90. **The effects of convection on chemical reactions and precipitation scavenging**
Neil R Gimson
July 1998

Met Office Joint Centre for Mesoscale Meteorology Department of Meteorology
University of Reading PO Box 243 Reading RG6 6BB United Kingdom
Tel: +44 (0)118 931 8425 Fax: +44 (0)118 931 8791
www.metoffice.com